Transient Free-Surface Flows: Motion of a Fluid Advancing in a Tube

The fluid motion at a free surface advancing into a mold or duct is appreciably different from its steady state behavior in well-developed flow; this affects the residence time distribution and structure of macromolecular fluids as they are frozen in injection molding processes. In this work such motion is treated numerically and measured precisely for Newtonian fluids. While the three-phase contact line represents a special problem conceptually and analytically, a very simple algorithm is seen to represent the fluid motion in this region accurately.

Good agreement is found over wide ranges of the governing dimensionless groups (the Reynolds, Jeffrey, and capillary numbers). Since viscous forces are dominant under the circumstances studied, this finding is not surprising but it confirms the applicability of the numerical methods developed herein to the modeling of these flows under conditions of actual interest. As a result, simulations may be made with confidence to predict flow patterns encountered in practice but difficult to reproduce in laboratory experiments.

R. A. Behrens, M. J. Crochet
C. D. Denson, A. B. Metzner
Center for Composite Materials and
Department of Chemical Engineering
University of Delaware
Newark, DE 19716

Introduction

Mold-filling operations in polymer processing are characterized by transient free-surface flows which can be classified conveniently using either of two flow scales, macroscopic or microscopic. Macroscopically, the Hele-Shaw flow approximation describes the overall behavior of the system and provides a relation between pressure drop, flow rate, and position of the leading edge of the fluid. From such computations one obtains mold filling times as functions of experimental variables such as the mold geometry and temperature, and the rheological properties of the fluid. This has been a major focus of molding simulations.

The ordering arguments used to define a Hele-Shaw flow are inapplicable near the free surface of the advancing liquid phase and along inserts and the side walls of the mold cavity. Yet it is in these regions that the velocity field is of great interest, controlling, as it does, the molecular structure and residual stresses in a molded polymeric object, and the orientation of suspended fibers when short-fiber composite solids are being molded. To elucidate these microscopic aspects of the flow one must consider a complex two-dimensional velocity field with as few simplifications as possible. The streamlines near an advancing fluid front appear like a fountain when viewed from a frame of reference that moves with the mean velocity of the fluid. The term "fountain flow," first coined by Rose (1961), refers to an outward trajectory of the fluid particles from the central region toward the bounding walls. The use of such a moving frame of reference is convenient for studying the isothermal flow in a straight-walled channel because the problem reduces to a steady-state free surface calculation. This insight has led to several contributions on fountain flow and these will be discussed below. However, many fountain-flow geometries cannot be considered to be straight-walled even if the walls of the cavity are straight; for example, an uneven geometry may develop from a freezing of the melt or from a reaction in the cavity, as in the case of reaction injection molding. The shape of the boundary changes with time in these examples, and the reduction to a steady-state technique is inapplicable. This reduction is also impossible for studying the microscopic flow of resin around individual fiber bundles in a resin transfer molding process and in any other process in which the mold contains inserts. In the present work we build a numerical algorithm for solving the fountain flow problem in an arbitrary geometry and careful experiments are carried out to validate the computed results.

Several types of geometries have been considered by Behrens

Correspondence concerning this paper should be addressed to A. B. Metzner.
R. A. Behrens is currently with Chevron Oil Field Research Co., La Habra, CA 90631.
The permanent address of M. J. Crochet is Mechanique Appliquee, B 1348, Louvain-la-Neuve, Belgium.

(1983). In the present paper, we will report on the transient, creeping, isothermal fountain flow of a Newtonian fluid in a circular cylindrical tube and in a channel with parallel walls. A step function in flow rate is applied, and one computes the velocity field, the pressure, and the shape of the moving front by means of a finite-element algorithm. These conditions faithfully reproduce the experiment used and hence provide for a valid comparison between theory and experiments.

Fountain flow

The literature on transient, viscous, free-surface flows is sparse. The contributions to fountain flow have mainly been made in simplified models or have described important aspects of the problem with simple descriptions or approximate analytical models. Battacharji and Savic (1965) considered the flow inside a tube of liquid being displaced by a piston whose facing is assumed to have no shear. For the free surface the authors assumed a flat interface with no shear. The problem was worked out in a moving reference frame and simplified for obtaining a compact approximate analytical solution. Tadmor (1974) has made a significant contribution by suggesting that one may model the centerline motion as a stagnation flow between parallel walls. The flow was considered fully developed until a fluid particle moved to within two half-gap distances of the front. The flow was then approximated as a planar stagnation flow with the velocity along the centerline descending linearly from its maximum to average levels:

$$d_{11} = (v_{max} - v_{ave})/2B = 0.25\ V/B \tag{1a}$$

where B is the half-gap thickness and V denotes the mean axial velocity. Tadmor noted that the elongational orientation would be perpendicular to the direction of flow except for the rolling action at the front, which moves the fluid along the approximate quarter-circle that constitutes one symmetric side of the front.

Corresponding to Eq. 1a for flow between parallel flat planes, one may write for the axisymmetric case of flow through a round tube:

$$d_{11} \approx 0.5\ V/B \tag{1b}$$

where B now denotes the tube radius.

A finite-difference numerical solution coupled with the marker and cell (MAC) technique has been used by Huang et al. (1978) for following the front progression in a fixed frame of reference. Kamal and coworkers (1985) used a similar numerical technique to study free-surface flows in a mold for a nonisothermal, viscoelastic power-law liquid, but focused primarily on the global effects of temperature, viscous dissipation, and the differences between the fluid and mold-wall temperatures.

Finite-element techniques may, however, be better suited for flow in complex geometries and may be used to represent the free surface more readily. Wang et al. (1978, 1979) have used these for calculating the steady front in a straight-walled channel. Their algorithm uses a kinematic boundary condition as the constraint for locating the free surface. This procedure allows for a limited amount of surface tension; other procedures compatible with high surface tension have been proposed by Silliman and Scriven (1980).

The evolution of the detailed deformation of material elements near the free surface of a fluid front advancing in a channel formed by parallel flat plates have been described numerically by Mavridis et al. (1986a) and by Coyle (1986). Mavridis et al. (1986b) have described the steady-state fluid mechanics of the fountain flow and show calculated velocity and pressure distributions of the front. The present work complements that study by focusing on transient aspects of the fluid motion and deformation processes both by numerical and experimental methods.

Numerical Technique

The geometry of the problem is shown in Figure 1. For the sake of simplicity, we will limit our description to the plane transient flow between parallel walls; the extension to axisymmetric flows is straightforward and it is this latter geometry that will be employed in the experimental verification of the numerical predictions. Plane Poiseuille flow is imposed in the entry section OA. There is no slip along the wall AC, while OB is a plane of symmetry. We solve the problem in a fixed frame of reference with respect to the wall AC. Thus, the free surface BC moves as a function of time. We wish to determine the shape of the free surface and the location of the contact line C as time progresses.

We consider the creeping flow of an incompressible Newtonian fluid. The planar Stokes equations are given by:

$$-\nabla p + \nabla \cdot (2\mu \boldsymbol{d}) + \boldsymbol{f} = 0$$
$$\nabla \cdot \boldsymbol{v} = 0 \tag{2}$$

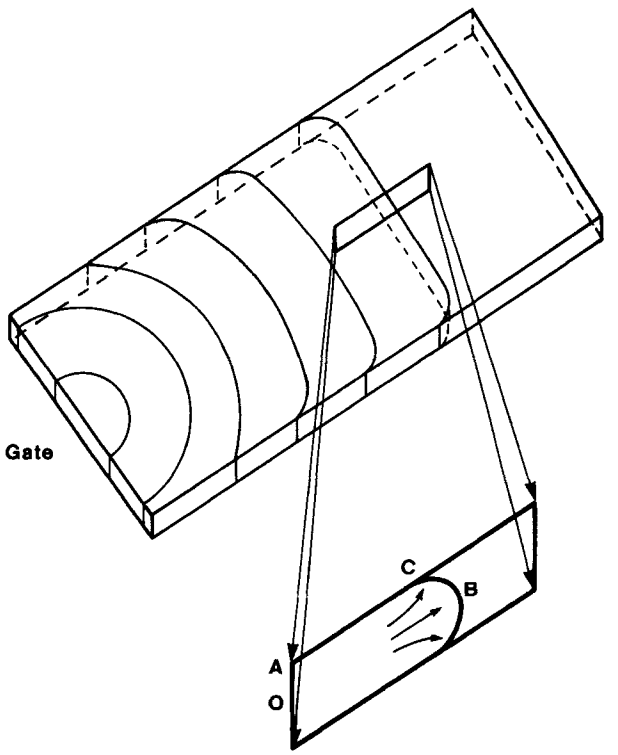

Figure 1. Macroscopic overview of molding with microscopic view inserted.

While the inertia terms can be omitted from the momentum equations in view of the creeping flow hypothesis, the motion of the free surface results in time-dependent velocity and pressure fields.

The boundary conditions imposed on the sides *OA*, *AC*, and *OB* are straightforward. Along the free surface, we impose a vanishing tangential surface force component, while the normal component is proportional to the local curvature of the free surface and the surface tension coefficient.

The flow domain is covered by a mesh of finite elements; we find it convenient to mix triangular and quadrilateral elements. We select the velocity components and the pressure as the unknown functions of the problem, together with the location of the free surface. For the velocity interpolation we use nine-node Lagrangian elements with biquadratic shape functions and six-node triangular elements with quadratic shape functions. The pressure is interpolated by means of bilinear shape functions on quadrilaterals and first-degree polynominals on triangles, respectively. Thus, the velocity field $\boldsymbol{v}$ and the pressure p are replaced by their respective finite-element representations $\boldsymbol{v}^*$ and p^*, which may be written as follows:

$$\boldsymbol{v}^* = \Sigma\, \boldsymbol{v}^i \psi_i,\ p^* = \Sigma\, p^i \phi_i, \tag{3}$$

where the $\boldsymbol{v}^i$ and p^i are nodal values while ψ_i and ϕ_i denote shape functions. The finite elements contained within the mesh are subparametric, i.e., they have straight edges, while they are isoparametric along the free surface *BC*. We will find below that the isoparametric formulation is an essential ingredient for calculating the motion of the contact line *C*.

The calculation starts at time $t = 0$ on a finite-element mesh that fits the imposed initial location of the free surface. As time progresses, the motion of the front requires a moving finite-element mesh. The algorithm may be decomposed into four parts, which consist of the calculation of the velocity and pressure fields at a given time, the motion of the free surface, the motion of the contact line, and the evolution of the finite-element mesh. Let us briefly consider each of these steps.

Calculation of velocity and pressure fields

We will find below that the calculation of the velocity and pressure fields is required at various stages of the algorithm. The presence of moving meshes does not complicate the calculation because the time derivative of the velocity field has been omitted in view of the creeping flow hypothesis. If it were present, the motion of the mesh would be taken into account by means of the procedure introduced by Lynch and Gray (1980). In this study the mesh deformed within the fluid domain but the nodal points did not move relative to the material.

The Stokes equations are discretized by means of the Galerkin formulation; the discretized equations read as follows,

$$\int_\Omega [(\nabla \psi_i^T) \cdot (2\mu \boldsymbol{d}^* - p^* \boldsymbol{I}) - \psi_i f]\, d\Omega = \int_{\partial\Omega} \psi_i \boldsymbol{E} d\mathrm{E},$$
$$\int_\Omega \phi_i \nabla \cdot \boldsymbol{v}^* d\Omega = 0, \tag{4}$$

where $\boldsymbol{d}^*$ is the rate of deformation tensor calculated on the basis of $\boldsymbol{v}^*$, $\boldsymbol{E}$ is the surface force applied on the part of the boundary where the velocity is not specified, and Ω designates the flow domain. Substituting Eq. 2 for $\boldsymbol{v}^*$ and p^* in Eq. 3, one obtains a linear algebraic system of equations in terms of the $\boldsymbol{v}^i$ and the p^i terms. More details on the finite-element formulation of a flow problem are given by Behrens (1983) as well as in a recent textbook (Crochet et al., 1984).

Motion of the free surface

The time scale is discretized into a set of finite time steps. For proceeding from time t_n to t_{n+1} we need to move the nodes located on the free surface for defining its new shape. The procedure, which is schematically presented in Figure 2, consists of the following steps:

1. The velocity field $\boldsymbol{v}_n$ is calculated on the basis of the mesh at time t_n.
2. For the nodes lying on the free surface, the velocity $\boldsymbol{v}_{n-1}$ at time t_{n-1}, is identified by means of an interpolation procedure, because the mesh has been transformed between times t_n and t_{n+1}.
3. The new positions of the nodes on the free surface are predicted by means of a second-order Taylor expansion

$$x^p_{n+1} = x_n + \Delta t_n [\boldsymbol{v}_n + \Delta t_n (\boldsymbol{v}_n - \boldsymbol{v}_{n-1})/(2\Delta t_{n-1})] \tag{5}$$

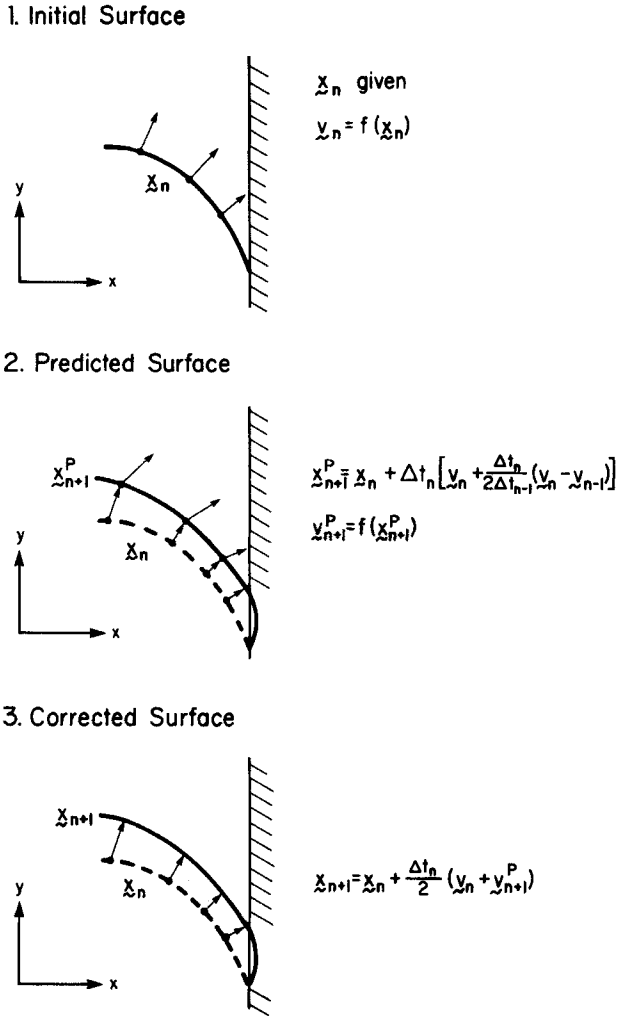

Figure 2. Use of finite-element predictor-corrector method for numerical calculations.

A first-order predictor is used for the first time step when the previous history is unavailable.

4. A predicted velocity field v^p_{n+1} is calculated on the basis of the updated free surface. (The predicted position of the contact point will be discussed below). The nodes inside the domain remain unchanged at this stage.

5. The corrected position at time t_{n+1} of the nodes lying on the free surface is then given by:

$$x_{n+1} = x_n + (v_n + v^p_{n+1})\Delta t_n/2. \quad (6)$$

The predictor-corrector algorithm is more accurate than a fully explicit scheme, with a truncation error of order Δt^3. A variable time step is used for controlling the truncation error as outlined by Gresho and coworkers (1980).

Motion of the contact line

A major conceptual difficulty of free-surface flow problems is that of locating the contact point C of Figure 1 at each time t_n. In contrast with the boundary conditions of the Hele-Shaw flow, the fluid does not slip along the wall in the present problem. Thus, if a node coincides with the contact point, its velocity vanishes and the procedure that we have adopted for the free surface would not allow for any motion of the contact line. The basic idea of the method used here is to find, at time t_n, that fluid material point, initially some (small) distance from the wall, which will just hit the boundary at time t_{n+1}. Then the position of that material point at time t_{n+1} will constitute the new contact point.

To this effect, we start from the free surface at time t_n, calculate all velocities at the same instant, and move the frontal nodes to their position at time t_{n+1} as depicted in the lower part of Figure 2. When the projected surface does not intersect the boundary at more than one place, we conclude that the contact line has not moved; however, once the projected surface intersects the boundary at another location, this new location becomes the new contact line. It is important to note that this method is based upon the use of quadratic shape functions for the velocity field and isoparametric elements along the boundary; it is not suitable for linear shape functions describing the element boundary because one could then not find an intersection unless the first node next to the boundary were projected onto it arbitrarily during the time step under consideration.

One measure of the accuracy of this method of determining motion of the contact line with the wall is to compute the volume of fluid that is transported (calculationally) through the solid wall and is lost. Because the transverse velocity is so small in the element nearest the wall, appreciably less than 0.01% of the fluid is lost in each time step. The size of the maximum time step is controlled largely by the size of the element nearest the wall; smaller time steps were taken during mesh refinement studies to verify convergence.

The dynamic contact angle at the wall is not specified in this procedure, it is calculated. Hoffman (1975) presents a shift curve to be applied to a static angle to calculate dynamic angles, but this technique was unnecessary in the present work because, for capillary numbers on the order of unity or higher, the static angle is completely overridden by viscous forces; it is this range of capillary numbers for which the present method was developed. The problem becomes much more difficult if the dynamic contact angle is influenced both by viscous forces and the static angle; a review of these problems has been given by Dussan (1979). In the method presented here the interfacial tension still may affect the fluid motion at the free surface, and the shape of this surface, even though there is no effect on the contact angle itself. However, none of the simulation results presented in this work included interfacial forces.

Construction of the finite-element mesh

The predictor step of the new free-surface calculation has little impact upon the finite-element mesh. Provided the time step is small enough, we can use the same mesh for the predictor and the corrector steps except that the coordinates of the free-surface nodes are slightly modified. Such a procedure cannot be used for more than a time step because otherwise all the initial free surface nodes would eventually lie on the boundary wall. Thus, after the completion of the corrector step, one needs to relocate the nodes of the free surface and of the straight walls and to design a new and well-behaved mesh. The procedure used for relocating the boundary nodes is discussed at length by Behrens (1983); for the fountain flow between parallel walls, one aims at a regular spacing along the front, while the spacing along the wall and the plane of symmetry increases from the front to the entry section.

The topology of the mesh, i.e., the type of elements and their relative positions, is established once and for all in a reference (ξ, ζ) frame. For each (ξ, ζ) pair in the standard mesh there corresponds an (x, y) pair in the actual mesh. It has been shown by Denayer (1980) that an appropriate mesh is built when the functions $x(\xi, \zeta)$ and $y(\xi, \zeta)$ are harmonic, i.e.,

$$\left(\frac{\partial^2}{\partial\xi^2} + \frac{\partial^2}{\partial\zeta^2}\right)x(\xi, \zeta) = 0, \quad \left(\frac{\partial^2}{\partial\xi^2} + \frac{\partial^2}{\partial\zeta^2}\right)y(\xi, \zeta) = 0 \quad (7)$$

Thus, for each remeshing step, one needs to solve Eq. 7 with Dirichlet boundary conditions, since the location of the nodes is imposed on the boundary. Figure 3 shows a typical example of the remeshing procedure; on the left we see the standard mesh, while the figure on the right shows the solution of Eq. 7 for a fixed set of boundary nodes. Additional care is needed for the location of the boundary nodes when the flow occurs in geometries more complex than that of either a channel formed by wide, parallel flat plates or a cylindrical tube.

Experimental Method

The transient fountain flow created by a step change in flow rate was studied in cylindrical tubes over a range of flow rates with two different fluids and with two tube diameters. In order to observe the flow, the tubes were made by drilling smooth holes having diameters of 1.59 and 3.18 mm into an optically clear acrylic block. A constant-flowrate pump was connected to this block and to a bypass line through which the fluid was discarded until the initial pump transients settled. Switching of the valve to close the bypass line and to open the ducting to these clear tubes enabled the initiation of the desired step change in flow rate.

Corn syrup with a Newtonian viscosity of 137 Pa · s and a polybutene oil, Chevron 32, with a viscosity of 82 Pa · s, were the fluids used. For clarity the oil was pigmented with a powdered black tempera paint. Care needed to be exercised to minimize heating by viscous dissipation; all flow studies were at the

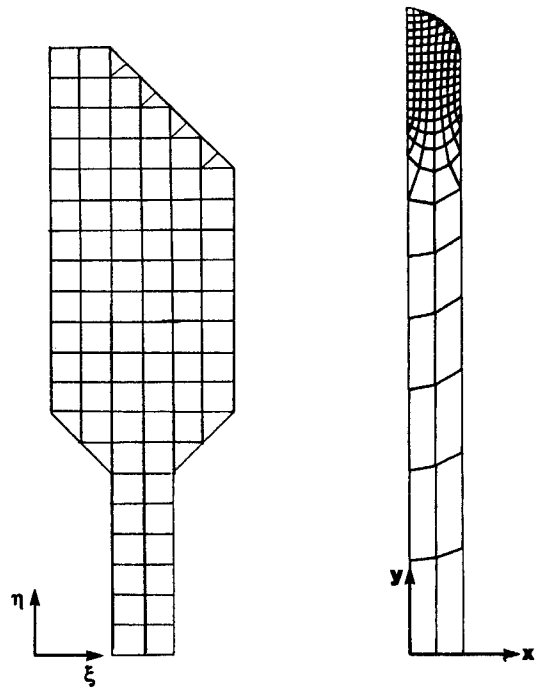

Figure 3. Grid evolution.
Initial mesh on left is reshaped into deformed mesh on right

295 K temperature at which the viscosity had been determined. Additionally, the high-intensity lights used to obtain clear photographs of the advancing fluid front were only switched on for a few seconds at a time in order to minimize the otherwise appreciable nonisothermal effects from this energy source. No normal stresses, or changes of viscosity with shear rate, were measurable with either fluid. Surface tensions were taken from handbook values; in actual molding operations, as in this study, the ratio of viscous to surface forces is large and the precision of the surface tension is not of great importance to us. Table 1 lists the conditions used and the corresponding values of the Reynolds, Jeffreys and capillary numbers. The capillary number (ratio of viscous to surface forces) is seen to be greater than unity in all but one case. The range employed is believed to include that found in the majority of molding applications. Since these capillary numbers are generally greater than unity, any skin effects, such as the surface wettability at the solid boundary, should be unimportant in both this work and in molding operations.

Table 1. Conditions of Fountain Flow Experiments

Fluid	Dia. mm	Veloc. mm/s	$Re \times 10^{+4}$ $\rho DV/\mu$	Je $\Delta\rho g D^2/\mu V$	Ca $\mu V/\sigma$	Asymp. Δy
Corn syrup	1.59	9.4	1.5	0.027	18.	0.858
	3.18	0.45	0.15	2.3	0.88	0.823
	3.18	1.0	0.32	1.0	2.0	0.856
	3.18	4.9	1.6	0.21	9.6	0.832
	3.18	11.0	3.6	0.092	22.	0.816
Polybutene	1.59	4.5	0.78	0.06	12.	—
	1.59	17.5	3.0	0.015	48.	0.815
	3.18	5.3	1.8	0.20	15.	0.824
	3.18	5.7	2.0	0.19	16.	0.824
	3.18	11.5	4.0	0.094	32.	0.814
	3.18	15.9	5.5	0.068	44.	0.791
					Average	0.83 ± .04

Corn syrup: μ = 137 Pa · s, ρ = 1,400 kg/m^3, σ = 0.070 N/m
Polybutene: μ = 82 Pa · s, ρ = 900 kg/m^3, σ = 0.030 N/m

The motion of the free surface was recorded photographically, using a Bolex H-16 (16 mm) movie camera equipped with a 100 mm lens and a 150 mm lens extension, over a range of speeds from 8 to 30 frames/s. Both Tri-X and Plus-X black-and-white reversal Kodak films were employed. The developed films were read with a frame analyzer, using reference marks on the acrylic wall of the channel to determine the locations of both the fluid centerline and the contact line at the wall as a function of time. The 36-fold magnification obtained allowed for high accuracy in locating the fluid front positions. The standard deviations of locating the contact line and the front were only 0.007 and 0.019 tube radii, respectively, or less than 2%. The portions of the free surface that could be distinguished most accurately were the leading tip and the contact line, and so it is these positions that were recorded for comparison with numerical simulation. Further details are available (Behrens, 1983).

Numerical Results

The calculated fluid motion, as the liquid advances upward in a vertical tube, is shown in Figure 4. The left side of the figure represents the axis of symmetry; the solid wall is on the right. Sixty time steps of magnitude $\Delta t\ddagger = 0.044$ were used to obtain the results for this figure. The relationship between $\Delta t\ddagger$ and the actual dimensional time increment is given by:

$$\Delta t = R\Delta t\ddagger / V_{ave} \tag{8}$$

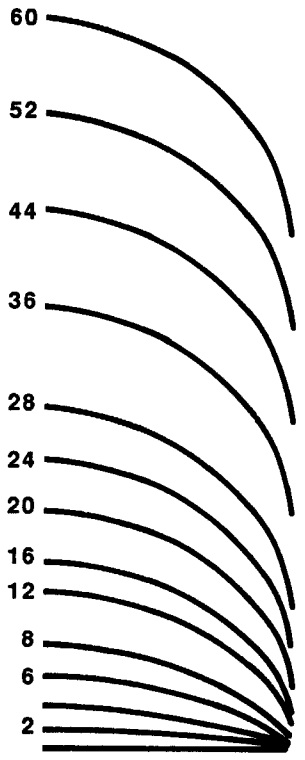

Figure 4. Computed profiles of transient axisymmetric fountain flow.
Numbers denote number of time steps $\Delta t\ddagger$ elapsed after initiation of flow

We note in Figure 4 that after four time steps the fluid has advanced appreciably upward in the tube at its centerline, but that the contact line at the wall has not moved at all. This stationary nature of the contact line is unrelated to any fluid-surface forces and is simply a consequence of the high level of the viscous forces within the fluid when the Reynolds number is much less than unity. As times increases further there is a net upward displacement of the fluid front at all radial positions, including that at the wall, and eventually the curves appear to become parallel to one another, indicating that a steady-state profile for the advancing front has been obtained.

With respect to later calculations of material residence time, temperature, and deformation state, it is important to note that the net upward motion does not imply that there is a positive vertical velocity component at all surface positions. The movement of the contact point is due to a spilling motion, and the fluid at the contact point remains fixed in space as the front leaves it behind. The steady state solution may be used to elucidate the rolling motion of the free surface more clearly: Figure 5a depicts the calculated streamlines for axisymmetric flow using, as the frame of reference moves, the average fluid velocity and hence the average frontal velocity. In such a frame of reference the centerline fluid moves upward and the wall itself moves downward. The spilling motion of the front is clearly seen: the axial velocity decreases from its initial value to zero as a material point passes from the region of fully developed flow toward the tip of the advancing front; it is then convected radially outward along the free surface where the velocity tangential to the path line of the material point increases monotonically. The translation out from the center toward the sides is very abrupt. The elongational contribution of both the centerline region and the region out along the free surface compresses the fluid in the original direction of flow and elongates it in the original transverse direction, which becomes nearly parallel to the wall as the fluid is laid down along the wall.

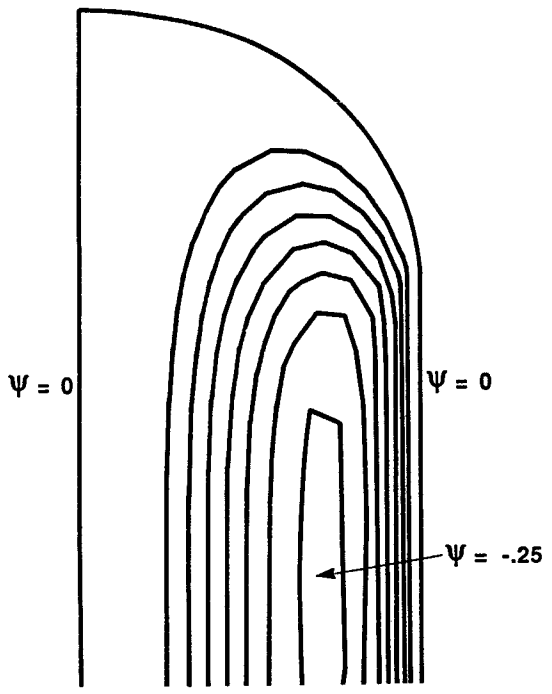

Figure 5a. Streamline contours for axisymmetric fountain flow.
Finite-element calculations using a moving frame of reference

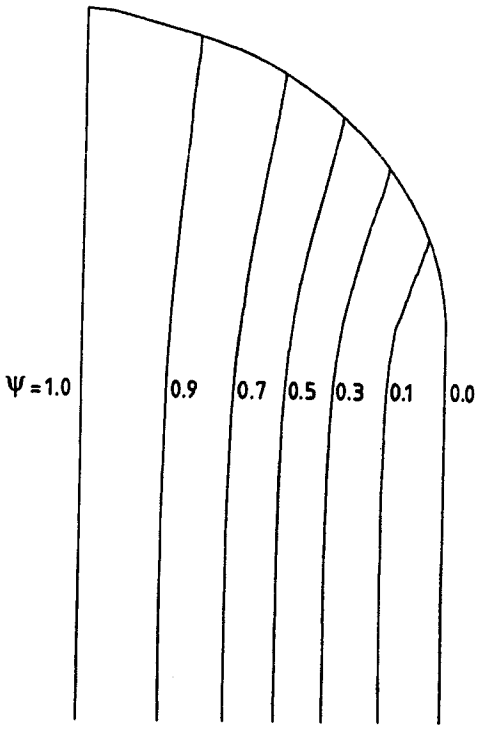

Figure 5b. Streamline contours for axisymmetric fountain flow.
Finite-element calculations using a fixed frame of reference

The spilling motion is less evident in the streamlines of Figure 5b. Here, the frame of reference is the mold wall so the fluid trajectory is primarily axial.

Results and Comparison with Simulation

To quantify the relative motion of various parts of the fluid and the time or distance required for a steady-state profile to be reached, we consider the actual upward distances travelled by the fluid at the centerline and at the wall. The difference between these two, Δy, is plotted v. the front travel—the axial distance between the centerline position at any time and its initial position—in Figure 6. Both Δy and the front travel have been divided by the tube radius, R, to render them dimensionless. Thus, when $\Delta y = 1.0$ the fluid front at the centerline lies on the arc of a circle of radius R and tangent to the wall at the contact point, and when $\Delta y = 0$ it is flat.

Figure 6 depicts the computed evolution of the fluid motion by the curve shown and the experimental measurements as discrete points. Every second or third measurement is shown in the regions in which many measurements overlap, while every data point is depicted in the regions in which data are scarcer. The first two data points, at $\Delta y = 0.034$ and 0.073, represent fluid motions at the centerline of only 0.027 and 0.12 mm, respectively. Even these extraordinarily small motions are seen to have been measured accurately and predicted precisely. In these early stages of the flow process the overall front moves ahead but the fluid at the wall remains stationary; under these conditions the slope of the curve is unity. At later stages in the flow process, when the contact line is also advancing, Δy represents a

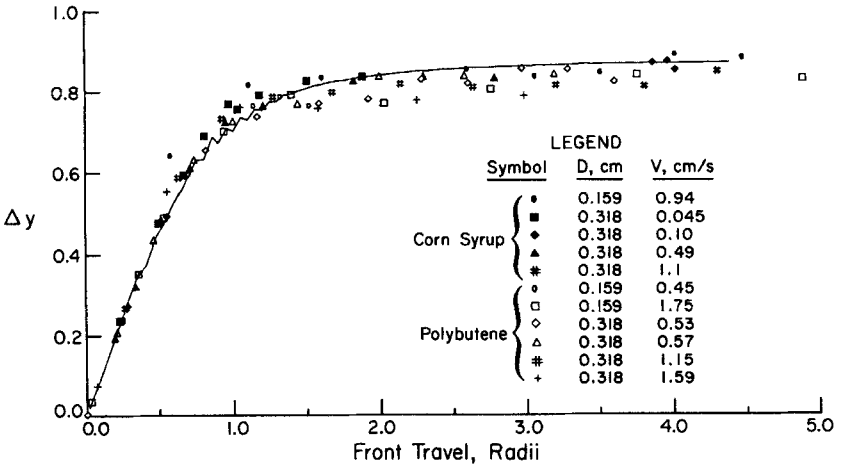

Figure 6. Transient axisymmetric front development.
Curve computed using finite-element method compared with experimental data

difference between two numbers and the experimental scatter appears greater. This is also affected by the fact that the actual contact line travel is dependent upon small experimental irregularities, such as those due to surface roughness and cleanliness. In spite of these variations, however, the overall behavior is well defined: there is no measurable motion at the wall until $\Delta y = 0.4$; it then increases gradually and a steady state value of $\Delta y = 0.83 \pm 0.04$ is reached after a front travel of about 1.5 radii; correspondingly, the computed curve becomes flat after a front travel of 2.5 radii. Table 1, which describes the experimental conditions in detail, shows that the Reynolds, Jeffreys, and capillary numbers were varied over 37-, 150-, and 55-fold ranges, respectively, in the course of this work.

The numerical simulation shown in Figure 6 depicts the data extremely well early in the motion, when the largest effects of a mismatch between experimental conditions and the assumed flow might have been expected. Slight oscillations arose in the Δy region between 0.6 and 0.8; reference to the detailed calculations shows that the oscillations all occurred in the computed motion of the contact line, not in the motion of the fluid front elsewhere. However, they never exceeded 2% of the asymptotic value and were self-stabilizing.

These same data are presented in another form in Figure 7 to clarify the difference between the motion at the fluid front and that at the wall. Here it is clearly seen that the contact line does not move at all until the front is appreciably developed, and then only slowly until the frontal development is substantially complete. Again, the agreement between the numerical predictions (solid line) and the experimental data is seen to be very good. The absence of fluid movement near the wall in the early stages of flow is reasonable physically in view of the low fluid velocities near the wall: when the contact line eventually does move it is because of a radial outflow from the partially developed (or fully developed) fluid front, not because of any rapid upward motion of fluid in the wall region. This perception as to the origin of fluid elements on the wall is important if, at a later stage, we wish to compute macromolecular or fiber orientations near the wall in an actual molding flow process.

The true value of Δy that should be reached asymptotically in these viscosity-dominated flows is not known *a priori*. The values computed by different techniques show considerable variations from each other, as summarized in Table 2, where we have included our own calculations for flow in a channel formed between two wide, parallel flat plates, as well as the results for

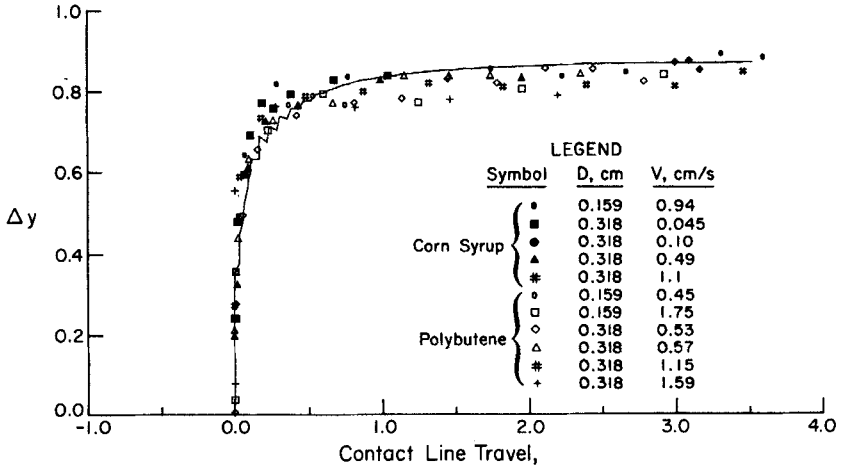

Figure 7. Computed and experimental development of the profile of advancing fluid front. The travel is expressed in tube radii.

Table 2. Asymptotic Frontal Development (Δy) Calculations for Planar and Axisymmetric Geometries

Investigator	Geometry	Frame of Ref.	Δy
Mavridis et al. (1986b)	Planar	Moving-steady	0.90
Wang et al. (1978)	Planar	Moving-steady	1.04
Wang et al. (1979)	Planar	Moving-steady	0.84
This work	Planar	Moving-steady	0.94
This work	Planar	Fixed-transient	0.91
Mavridis et al. (1986b)	Axisym.	Moving-steady	0.83
This work	Axisym.	Moving-steady	0.82
This work	Axisym.	Fixed-transient	0.86
This work	Axisym.	Exp. result	0.83 ± 0.04

flow through a tube. We have shown (Behrens, 1983) that further mesh refinements in our work do not change Δy values reported here. The steeper profiles found for the planar case suggest that appreciable differences in fluid orientation near the wall to arise between the two geometries; these were not anticipated intuitively.

Figure 5b shows computed streamlines for the axisymmetric (tubular) flow. We can see that the fluid entering the front along the centerlines appears to undergo a stagnation flow, that is, the streamlines diverge as the front is approached. Consequently, fluid elements are compressed as the particles slow down from the fully developed maximum velocity to the average velocity at the front. This observation is depicted quantitatively in Figure 8, in which the computed tangential velocities and deformation rates along the centerline flow path are shown. The abscissa used in this figure (as well as for the corresponding Figure 9 for the planar flow) represents positions, measured in tube radii, upstream from the centerline of the front for negative values of the ordinate. In Figure 9 positive values of the ordinate denote positions along the trajectory of the centerline fluid element as it moves outward radially along the front towards its destined location on the surface of the duct.

Figures 8 and 9 show that the axial compression of a fluid element, as measured by its decrease in velocity, begins about 1.8–

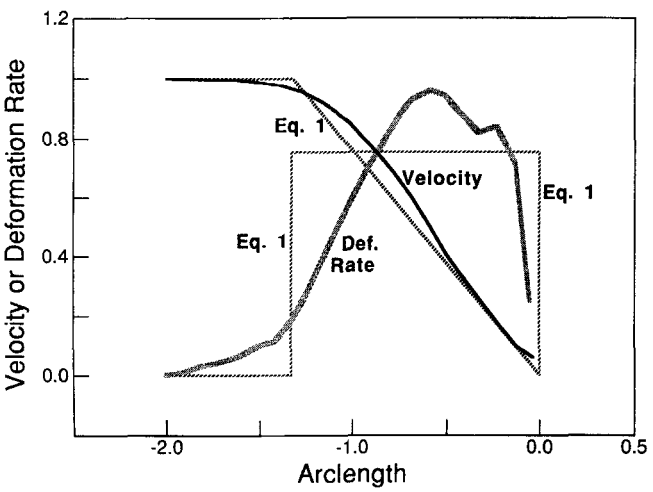

Figure 8. Evaluation of "stagnation flow" approximation for axisymmetric fountain flow.
The abscissa refers to position along the center line in radii.
Predictions from Eq. 1 include adjusted constants; see text.

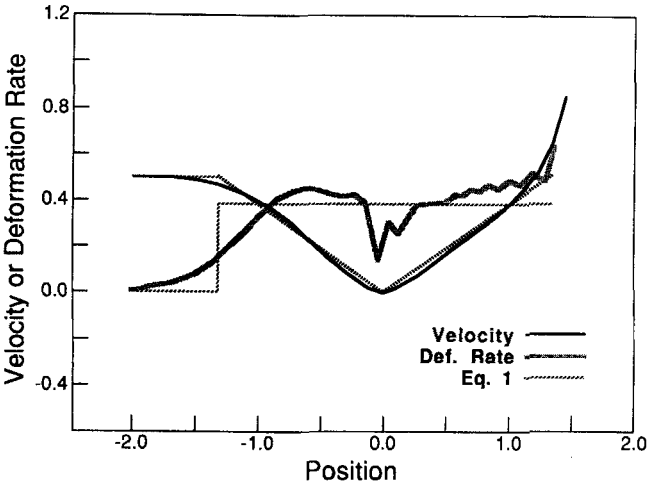

Figure 9. Evaluation of "stagnation flow" approximation for planar fountain flow.
Legend and abscissa as in Fig. 8.
Predictions from Eq. 1 include adjusted constants; see text.

2.0 radii behind the front. About one radius behind the front this velocity decrease rate appears to have become almost perfectly linear, i.e., the fluid deformation rates have become nearly constant. The computed deformation rates reveal that while this is not truly so, the Tadmor model, Eq. 1, shown as dotted lines, is a remarkably accurate depiction of the process provided that the constants in Eq. 1 are adjusted upward from values of 0.25 and 0.50 to 0.38 and 0.75, respectively. This stagnation approximation for the velocity in Figure 9, the case considered by Tadmor, appears to hold reasonably well until the material element reaches the last third of the free surface, when shearing begins. Near the contact point with the wall, at an axial position of about +1.5 in Figure 9, the finite-element simulation breaks down because of the assumption of an instantaneous change from a finite velocity to zero as a fluid element strikes the wall.

Conclusions

A numerical algorithm has been developed for the transient motion of a liquid over a solid boundary. The algorithm has been used for simulating the experimental creeping flow of a Newtonian fluid when gravity plays no role. The numerical calculations have produced results that show good agreement with experimental data. The algorithm allows superposition for different flow rates, diameters, and surface tensions over the very wide range of capillary, Jeffreys, and Reynolds numbers enumerated earlier. The agreement between numerical prediction and experiment is significant because some earlier attempts to model free-surface flows gave appreciably different results.

Most of the transient free-surface character of the flow in the advancing fluid is confined to about ½ of a tube radius as noted in Figure 5b for the axisymmetric case, and ⅔ of a duct half-width for the planar case. This means that the flow can be treated as being fully developed at all further upstream positions in these simple geometries. It also implies that in the case of flow through ducts of changing cross section or of fluid through a mat of fibers, the problem will have to be treated as a fully transient one whenever appreciable changes in flow geometry occur on a scale smaller than this.

The work validates (with slight adjustment of an empirical

parameter) the Tadmor approximation for fountain flow of a Newtonian fluid. In polymer processing operations the fluids are not Newtonian, of course, but at typical mold filling rates and temperatures the viscoelastic effects will frequently not be large.

Notation

B = half-spacing of flow channel
d = rate of deformation tensor
D = tube diameter
f = body force
g = gravitational acceleration
I = identity tensor
p = isotropic pressure
R = radius of flow tube
v = velocity vector
V = mean velocity
t = time
t = surface force vector
x = global coordinate
y = global coordinate
Δy = difference between frontal and contact point locations

Greek letters

μ = shear viscosity
ξ, ζ = local coordinates
ρ = density
σ = surface tension
ϕ = bilinear shape function
ψ = biquadratic shape function
Ω = domain of integration

Subscripts

i = local node number
n = time step n
T = transpose
ave = average
max = maximum

Superscripts

i = local node number
$*$ = finite-element approximations to local values
p = predicted but not yet corrected
$\ddagger$ = dimensionless variable

Literature cited

Behrens, R. A., "Transient Domain Free-Surface Flows and their Applications to Mold Filling," Ph.D. Diss. Univ. Delaware, Newark, DE (1983).

Bhattacharji, S., and P. Savic, "Real and Apparent Non-Newtonian Behavior in Viscous Pipe Flow of Suspensions Driven by a Fluid Piston," *Proc. Heat Trans. Fluid Mech. Inst.*, 248 (1965).

Coyle, D. J., "The Kinematics of Fountain Flow in Injection Molding," Polymer Proc. Soc. Meet. (1986).

Crochet, M. J., A. R. Davies, and K. Walters, *Numerical Simulation of Non-Newtonian Flow*, Elsevier, Amsterdam (1984).

Denayer, A., "Automatic Generation of Finite-Element Meshes," *Comp. Struct.*, **9**, 359 (1980).

Dussan V, E. B., "On the Spreading of Liquids on Solid Surfaces: Static and Dynamic Contact Lines," *Ann. Rev. Fl. Mech.*, **11**, 371 (1979).

Gresho, P. M., R. L. Lee, S. T. Chan, and R. L. Sani, "A New Finite-Element Technique for Boussinesq Fluids," *Proc. 3rd Int. Conf. Finite Elements in Flow Problems*, Banff, Canada (1980).

Hoffman, R. L. "A study of the Advancing Interface. I: Interface Shape in Liquid-Gas Systems," *J. Colloid Interf. Sci.*, **50**, 228 (1975).

Huang, C. F., C. G. Gogos, and L. Schmidt, "Cavity Filling, Including the Fountain Effect in Injection Molding," 71st Ann. AICHE Meet. (1978).

Kamal, M. R., E. Chu, P. G. Lafleur, and M. E. Ryan, "Computer Simulation of Injection Mold Filling for Viscoelastic Melts with Fountain Flow," Soc. Plastics Eng. Ann. Tech. Meet. (1985).

Lynch, D. R., and W. G. Gray, "Finite-Element Simulation of Flow in Deforming Regions," *J. Comput. Phys.*, **36**, 135 (1980).

Mavridis, H., A. N. Hrymak, and J. Vlachopoulos, "Deformation and Orientation of Fluid Elements Behind an Advancing Flow Front," *J. Rheol.*, **30**, 555 (1986a).

———, "Finite-Element Simulation of Fountain Flow in Injection Molding," *Polym. Eng. Sci.*, **26**, 449 (1986b).

Rose, W. R., "Fluid-Fluid Interfaces in Steady Motion," *Nature*, **191**, 242 (1961).

Silliman, William, and L. E. Scriven, "Separating Flow Near a Static Contact Line: Slip at a Wall and Shape of a Free Surface," *J. Comp. Phys.*, **34**, 287 (1980).

Tadmor, Z. "Molecular Orientation in Injection Molding," *J. Appl. Polym. Sci.*, **18**, 1752 (1974).

Wang, K. K., et al., "Computer-Aided Injection Molding System," Report 5, Cornell Univ. (1978).

———, "Computer-Aided Injection Molding System," Report 6, Cornell Univ. (1979).

Manuscript received Aug. 8, 1986, and revision received Jan. 9, 1987.